FAILURE MODE SCALING TRANSITIONS IN RC BEAMS IN FLEXURE: TENSILE, SHEARING, CRUSHING

A. CARPINTERI*, M. CORRADO* AND G. VENTURA*

* Politecnico di Torino
Department of Structural, Geotechnical and Building Engineering
Corso Duca degli Abruzzi 24, 10129 Torino, Italy
e-mail: alberto.carpinteri@polito.it – mauro.corrado@polito.it – giulio.ventura@polito.it

Key words: bridged crack model, cohesive crack model, crushing failure, ductility, shear failure, size effects.

Abstract: Reinforced concrete beams in flexure exhibit three different collapse mechanisms by varying the mechanical and geometrical parameters. The limit cases are: tensile failure for low steel percentages and/or small and slender beams, and crushing failure for high steel percentages and/or large and stocky beams. The intermediate collapse mechanism, and, therefore, the most frequent, is represented by diagonal tension failure, in which the collapse is dominated by unstable propagation of one or more shear cracks. In this paper, a study of the transitions between these mechanisms is proposed inside the theoretical framework of fracture mechanics. Relevant results concern the prediction of the predominant collapse mechanisms, the failure load as well as the analysis of the mutual transition between the different failure modes by varying the scale, the slenderness and the reinforcing steel amount. Then, other specific aspects are also investigated, such as the problem of minimum reinforcement necessary to prevent the phenomenon of hyper-strength at low steel percentages, and the rotational capacity of plastic hinges. Both these aspects, also affected by size-scale effects, have practical implications in defining structural elements with ductile response, as required by current design codes.

1 INTRODUCTION

The problem of determining the carrying capacity and the transition between the different failure modes within a unique consistent theoretical framework is of fundamental importance for the design of reinforced concrete (RC) beams. In the absence of stirrups, the three typical failure mechanisms are: flexure, diagonal tension, and crushing. They are usually treated separately, and, especially for what concerns the shear capacity, the most common Standard provisions seem to be too much conservative with respect to the experimental results. Shear crack propagation and diagonal tension failure have been addressed in the literature by several authors with different approaches. For example, some analyses with cohesive crack modeling have been published by Gustafsson and Hillerborg [1], and Niwa [2]. In the framework of linear elastic fracture mechanics some contributions were given by Jenq and Shah [3], and by So and Karihaloo [4].

On the other hand, the ultimate strength is not the only requirement to be fulfilled in the structural design. Among others, the ductility at the ultimate conditions is a fundamental characteristic to be guaranteed. It is related to the formation and the development of plastic hinges typical of RC beams reinforced with stirrups in order to prevent the shear failure. In particular, the longitudinal reinforcement amount has to be such as to prevent unstable crack propagation (lower bound) and to avoid brittle failure due to concrete crushing without steel yielding (upper bound). Significant contributions to the analysis of the minimum reinforcement and the rotational capacity can be found in ref. [5-11].

In the present paper, all the aforementioned aspects are analyzed within a fracture mechanics framework. First, a unified general model is proposed to study the transition between failure modes in RC beams without stirrups. It is an extension of the bridged crack model originally proposed by Carpinteri [12, 13] for the flexural mechanism, to encompass also diagonal tension and crushing failure [14]. The model is analyzed by showing the influence of the nondimensional parameters variation on the mechanical response and a global failure mode transition scheme is introduced. Then, the upper and lower bounds for a ductile behavior are analyzed, by investigating the minimum reinforcement amount and the rotational capacity of RC hinges. In these cases, the material nonlinearities play an important role, and, therefore, a numerical model based on nonlinear fracture mechanics is proposed [15, 16].

2 MODELLING FLEXURAL AND SHEAR CRACKS

A linear elastic fracture mechanics based approach is proposed to study the transition between the different failure modes in RC beams [14]. A family of crack paths is considered and, for each one, the stability of the fracturing process and the load required to activate it is evaluated. Then, the minimum load giving unstable crack propagation is assumed as the failure load and the corresponding crack path as that determining the collapse mechanism.

Consider a cracked beam, Fig. 1, and assume a crack propagation condition ruled by the comparison of the stress-intensity factor (SIF) K_I to the concrete toughness K_{IC}. While handbooks [17] report LEFM solutions for Mode I (bending) fracture, in the case of Fig. 1 no SIFs data are available and approximate expressions have to be used.

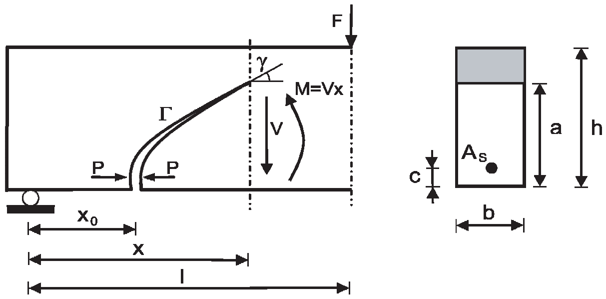

Figure 1: Cracked beam.

In Fig. 1 all the used symbols are defined: the section width b and height h, the crack tip vertical and horizontal positions a and x, the crack mouth horizontal position x_0, and the shear span l. The corresponding dimensionless quantities are introduced, after dividing by the beam height h the vertical distances and by the shear span l the horizontal distances, obtaining the parameters $\alpha = x/l$, $\alpha_0 = x_0/l$, $\xi = a/h$, $\zeta = c/h$, and $\lambda_l = l/h$.

The crack trajectory Γ is split into two parts: a vertical segment Γ_1 extending from the bottom to the reinforcement layer, and a power-law curve Γ_2, going from the end of the first part (reinforcement layer) to the loading point. Its analytical definition is:

$$\alpha(\zeta,\xi) = \begin{cases} \alpha_0 & 0 \le \xi \le \zeta \\ \alpha_0 + \left(\dfrac{\xi - \zeta}{1-\zeta}\right)^{\mu} (1-\alpha_0) & \zeta \le \xi \le 1 \end{cases} \tag{1}$$

Note that the peculiarity of the present approach, compared to the literature, is that the crack initiation point will be determined by analyzing the crack propagation process stability, while the shape is modeled by the parameter μ based on experimental results, as discussed in Section 3.2.

With reference to Fig. 1, let K_I be the SIF at the crack tip, given by the sum of K_{IV} due to the bending moment associated to the shear force V, and K_{IP}, due to the closing force applied by the reinforcing bars. The crack propagation condition reads:

$$K_I = K_{IV} - K_{IP} = K_{IC} \,. \tag{2}$$

The expression for K_{IV} is approximated by assuming that it can be evaluated by the SIF of a beam with a straight vertical crack subjected to the bending moment at the section where the crack tip is located:

$$K_{IV} = \frac{Vl\alpha(\zeta,\xi)}{h^{3/2}b} Y_M(\xi) = \frac{V}{h^{1/2}b} Y_V(\zeta,\xi)\lambda_l\,, \tag{3}$$

function Y_M being given by handbook solution [17]. Analogously, an approximate expression for the SIF K_{IP} at the crack tip due to the reinforcement reaction P is derived from the case of a vertical straight crack. Several numerical analyses by boundary elements [18] have been performed to evaluate the SIF for different positions of the crack tip. It is observed that the SIF is mainly a function of the angle γ defined in Fig. 1 and that K_{IP} can be approximated as:

$$K_{IP} = \frac{P}{h^{1/2}b} Y_P(\zeta,\xi)\beta(\gamma) = \frac{P}{h^{1/2}b} Y_{P_\gamma}(\zeta,\xi)\,, \tag{4}$$

where, given γ in degrees, by a nonlinear data fit it is:

$$\beta(\gamma) = \left(\frac{\gamma}{90}\right)^{0.2}, \tag{5}$$

and $Y_{P_\gamma} = Y_P(\zeta,\xi)\beta(\gamma)$. Function $Y_P(\zeta,\xi)$ can be found in fracture mechanics handbooks [17]. Therefore, by accurate numerical analyses, the exact values for the SIFs were evaluated, validating Eq. (3) and allowing to define Eq. (4) by data fitting. Let $\rho=A_s/bh$ be the reinforcement percentage referred to the entire cross section and

$$N_P = \frac{\sigma_y h^{1/2}}{K_{IC}}\rho \tag{6}$$

the brittleness number defined by Carpinteri [12]. Substituting Eqs. (3) and (4) into Eq. (2) provides:

$$\tilde{V}_F = \frac{1}{\lambda_l Y_V(\xi)}\left[1 + N_P \tilde{P} Y_{P_\gamma}(\zeta,\xi)\right], \tag{7}$$

where

$$\tilde{V}_F = \frac{V_F}{K_{IC}h^{1/2}b}\,, \tag{8}$$

$$\tilde{P} = \frac{P}{P_P}\,, \tag{9}$$

and P_P is the reinforcement traction limit. A rigid-plastic constitutive equation is assumed for the reinforcement, ruled by the stress σ_y, defined as the minimum between the yielding and the sliding stress for the bars [13]. Then $P_P=A_s\sigma_y$, where A_s is the reinforcement area. Equation (7) gives the shear of crack propagation as a function of the bar traction stress, σ_s, depending on the crack opening w at the reinforcement, that, in its turn, is given by the two contributions of the shear V and the bar reaction P. According to the rigid-perfectly plastic assumption, it is w=0 up to the yielding or slippage of the reinforcement, so that a displacement compatibility condition allows to determine P as a function of V. It follows that, if $P<P_P$ it is:

$$\tilde{V}_F = \frac{1}{\lambda_l\left[Y_V(\xi) - \dfrac{Y_{P_\gamma}(\zeta,\xi)}{r''(\zeta,\xi)}\right]}, \tag{10}$$

whereas, if $P=P_P$, it is:

$$\tilde{V}_P = \frac{1}{\lambda_l Y_V(\xi)}\left[1 + N_P Y_{P_\gamma}(\zeta,\xi)\right]. \tag{11}$$

The beam behavior up to failure is described in the present model assuming as control parameter the crack depth, that is the only monotonically increasing quantity in the process.

In the proposed approach, the crushing collapse is determined by the achievement of the compressive strength, σ_c, at the beam extrados. According to the linear elastic fracture mechanics approach followed in the derivation of the present model, the stress at the uppermost edge of the cracked section is evaluated, by the superposition principle, as the sum of the two following contributions:

$$\sigma^V = \frac{M}{bh^2} Y_\sigma^M(\xi) = \lambda_l \frac{V}{bh} Y_\sigma^V(\xi)\,, \tag{12}$$

$$\sigma^P = -\frac{P}{bh} Y_\sigma^P(\zeta,\xi)\,, \tag{13}$$

where $Y_\sigma^V(\xi)$ and $Y_\sigma^P(\zeta,\xi)$ are two functions numerically determined by means of adaptive finite element computations on cracked sections and nonlinear regressions [18]. The shear value for which $\sigma=\sigma_c$ is, in nondimensional form:

$$\tilde{V}_C = \frac{1}{\lambda_l Y_\sigma^V(\xi)}[N_C + N_P \tilde{P} Y_\sigma^P(\zeta,\xi)], \tag{14}$$

where N_C is a brittleness number for the crushing failure, defined as:

$$N_C = \frac{\sigma_c h^{1/2}}{K_{IC}}. \tag{15}$$

3 TRANSITION BETWEEN DIFFERENT FAILURE MODES

3.1 Modeling predictions

The proposed model covers the three fundamental failure mechanisms of RC beams: steel yielding (flexural), diagonal tension (shearing), and concrete crushing. The transitions between the aforementioned mechanisms are ruled by the nondimensional parameters N_P, N_C and λ_l.

Fig. 2 shows four $\tilde{V}_F$ vs. ξ diagrams obtained by increasing the brittleness number from 0.2 to 1.0 and letting λ_l=2.5, ζ=0.1, and μ=6. A sketch illustrating the crack trajectories at failure is reported for each beam model.

In Fig. 2a, when the nondimensional shearing force reaches a value of 0.14, the flexural crack (α_0=1.00) begins its stable growth. As the load is increased, some other stable neighboring cracks develop. The marked lines in the plot represent the growing cracks. When the nondimensional shearing force is equal to 0.18, the steel yields at the flexural crack: we assume that this value represents the flexural failure load. When the brittleness number is increased to 0.30 (Fig. 2b), the beam collapses by flexural failure at the mid-span crack, although an increment in nondimensional shearing force from 0.18 to 0.25 is observed and new neighboring cracks develop. If the brittleness number is increased to 0.40 (Fig. 2c), flexural and diagonal tension failure occurs at the same load level. In fact, the minimum of the maxima of the crack propagation curves coincides with the slope discontinuity (yielding) of the curve for α_0=1.00 (central crack). For higher values of the brittleness number (Fig. 2d) flexural failure needs a higher shear (α_0=1.00, $\tilde{V}_F=0.80$) than diagonal tension failure (α_0=0.60, $\tilde{V}_F=0.33$). Therefore, as N_P is increased, the failure mode shows a transition, from flexural to shearing.

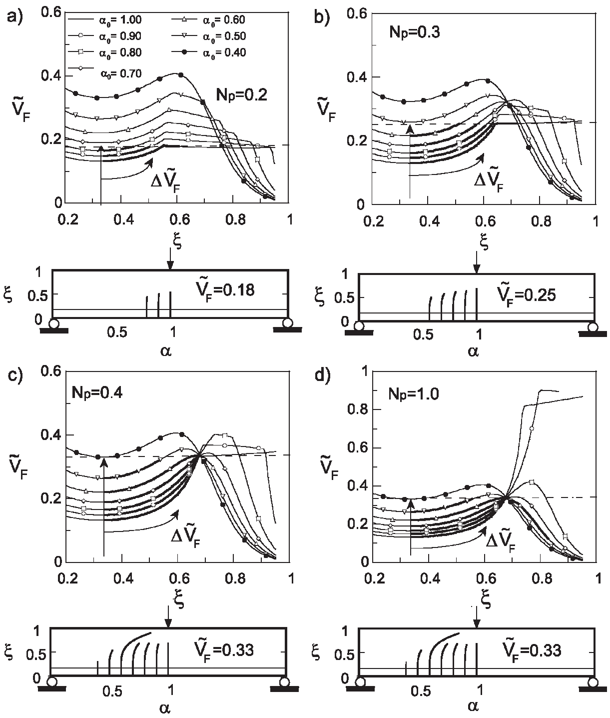

Figure 2: Transition from flexural to diagonal tension failure by varying N_P.

Figure 3 shows a sketch of all the failure mode transitions in RC elements. An increase in the number N_P, can be interpreted as: (1) an increase in the reinforcement area, transition *d-e*; (2) a decrease in the scale with constant reinforcement area, transition *a-e*; (3) an increase in the scale with a constant reinforcement percentage, transition *g-e*.

To discuss the right-hand side of the transition diagram in Fig. 3, crushing failure is to be considered and the behavior depends on the parameters N_P, N_C and λ_l. In Fig. 4a, the transition is shown by varying N_P. The shear $\tilde{V}_F$ at yielding increases with N_P (points A, D). The transition from flexural to crushing failure is apparent in Fig. 4a: for N_P=0.2 yielding precedes crushing, while for N_P=0.6 crushing precedes yielding. In Fig. 4b the transition can be observed from the nondimensional failure shear, $\tilde{V}_F$, of the two mechanisms. For low values of N_P, failure is by steel yielding. For N_P≅0.3, the transition takes place and the load-carrying capacity corresponding to crushing failure is lower. Physically, this transition appears when the reinforcement ratio ρ is increased and the remaining parameters are kept constant: we have the transition *e-f* in the scheme of Fig. 3.

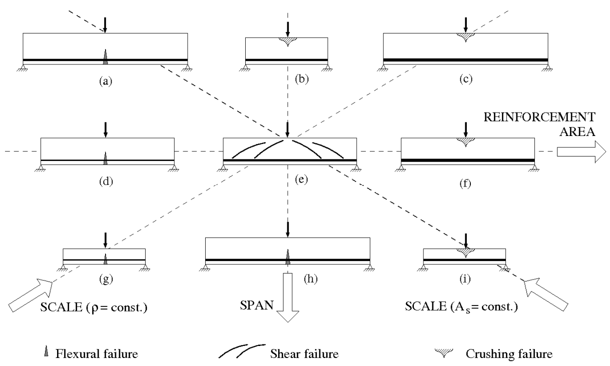

Figure 3: Global scheme illustrating failure mode transitions.

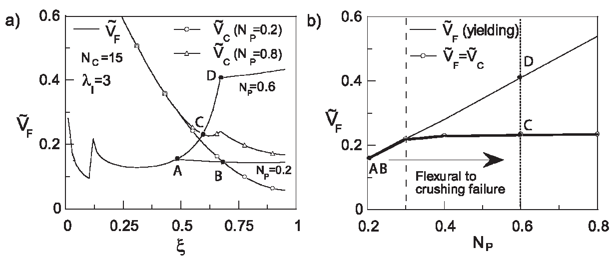

Figure 4: Transition from flexural to crushing failure: (a) $\tilde{V}_F$ vs. ξ; and (b) $\tilde{V}_F$ vs. N_P.

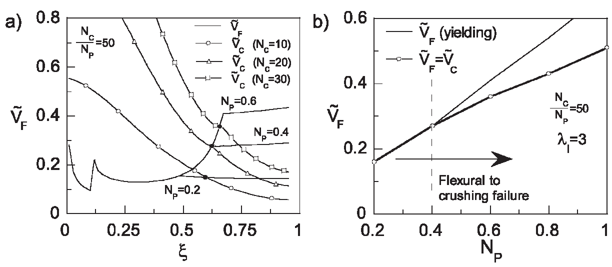

Figure 5: Transition from flexural/shearing to crushing failure assuming ratio N_P/N_C=50: (a) $\tilde{V}_F$ vs. ξ (black dots representing collapse load); and (b) $\tilde{V}_F$ vs. N_P.

Another transition can be shown as the beam is scaled keeping ρ constant (transition *g-e-c* in Fig. 3). By the definitions of N_P and N_C, this condition can be expressed by a constant ratio N_C/N_P. Curves for N_C/N_P=50 are reported in Fig. 5. For the ratio being constant, increasing N_P implies increasing N_C: therefore, both the loads for flexural/shearing collapse (controlled by N_P) as well as the load for crushing collapse (controlled by N_C) increase, although with different rates (Fig. 5b) and the failure mode transition occurs at N_P≅0.4.

Finally, the analysis of the size effect in the hypothesis that the reinforcement area A_s is constant, implying the ratio N_C/N_P being proportional to the cross section height h, permits the transition *a-e-i* in Fig. 3 to be represented.

3.2 Experimental evidences

An experimental program was carried out to study the influence of the reinforcement ratio on the crack pattern in RC beams [20] with height h=0.2 m and width b=0.1 m. The shear span slenderness ratio, λ_l, is equal to 3. Four different amounts of steel reinforcement have been considered: 1ϕ8 (ρ=0.25%), 2ϕ8 (ρ=0.50%), 2ϕ12 (ρ=1.13%), and 2ϕ20 (ρ=3.14%). They have been selected in order to examine all the most significant failure modes (yielding, shearing, crushing). Steel and concrete mechanical properties can be evinced from ref. [20].

The test setup for all beam specimens was three point bending. The mid-span deflection was chosen as control parameter in the tests. The load, F, and the deflection under the load point, δ, were continually monitored and recorded. Finally, the crack pattern on both sides of each specimen was acquired by high resolution digital photographs. For each reinforcement percentage, four specimens were tested.

All the experimental load vs. deflection curves for the reinforced beams are plotted in Fig. 6. The behavior of the beams is almost linear up to the cracking load. For the beams with the lowest reinforcement ratio, the cracking load almost coincides with the ultimate load. As the reinforcement ratio increases, a change in the initial slope appears. Depending on the reinforcement ratio, two different behaviors after the cracking load are observed. In the case of the reinforcement ratios 0.25% and 0.50%, the reinforcement yields and the load remains approximately constant with increasing deflection and ductile failure occurs. For beams with reinforcement ratios 1.13% and 3.14%, a sudden decrease in the loading capacity is measured with no steel yielding and a brittle crushing failure mode occurs.

The crack pattern is highly influenced by the reinforcement percentage. More in details, for low reinforcement percentages (0.25% and 0.50%), the steel yields very early in a crack and the overall cracking pattern is very limited. For the intermediate reinforcement percentage (1.13%), flexural and shear-flexural cracks appear along the span. Failure is generated by an unstable crack growth process: the reinforcing steel bars do not exhibit yielding and a sudden, brittle collapse takes place. Finally, for the beams with the highest reinforcement ratio (3.14%), the most extended crack pattern is observed. Flexural and flexural-shear cracks appear along the span and the cracking process develops until a concrete crushing failure occurs, characterized by the typical wedge-shaped crack near the load application point.

Although with increasing reinforcement ratios concrete cracking spreads all over the beam, attention is devoted to the determination of initial location and shape of the crack whose opening finally determines the beam failure (critical crack) in relation to the reinforcement percentage. The experimental critical cracks have been interpolated with the crack shape assumed in Eq. (1). Fig. 7 shows the critical crack trajectories observed on each tested beam and reported in a nondimensional diagram. Half of the beam is represented. The arrow in each plot indicates the load application point and the support is at the abscissa $\alpha_0=0$. From each test result, a nonlinear regression was performed to obtain the nondimensional parameters α_0 and μ defining the crack trajectory. The influence of the reinforcement ratio ρ on the nondimensional critical crack mouth position α_0 is described by the following empirical law:

$$\alpha_0 = 0.57 + \frac{0.10}{0.19 + \rho^{1.58}}\,. \qquad (16)$$

As the reinforcement ratio increases, the value of α_0 decreases, i.e. the critical crack originates closer to the support. It can be observed that, when the reinforcement ratio increases, the initiation point of the critical crack approaches the value 0.50, i.e. the critical crack develops near the central part of the shear span. Equation (16) is useful to provide the critical crack initiation coordinate, α_0, that can be compared to the one predicted by the model proposed in the previous section.

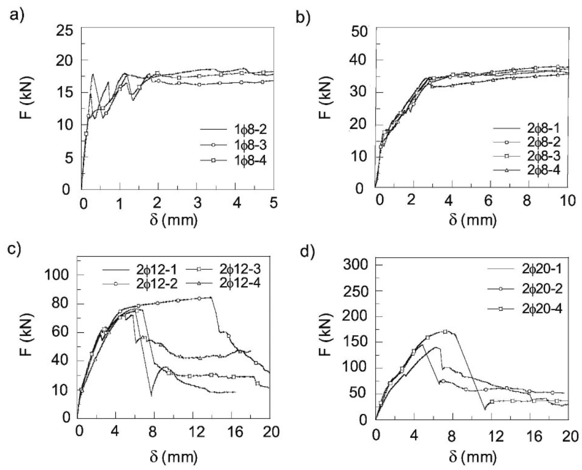

Figure 6: Experimental load-displacement curves.

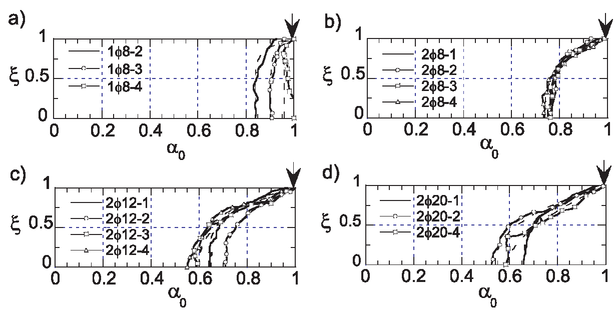

Figure 7: Critical crack paths.

The crack path exponent μ is defined by nonlinear regression of the digitized crack trajectories for each reinforcement percentage, assuming a law that best-fits the experimental results. The exponent tends to be smaller as the reinforcement ratio increases. This is a consequence of a smaller inclination of the critical crack with respect to the beam axis as the reinforcement percentage increases. The obtained nonlinear regression curve showing the data trend is:

$$\mu = 2.85 + \frac{0.27}{\rho^{2.71}}. \tag{17}$$

The experimental nonlinear regression data, Eqs. (16) and (17), as well as the used geometrical and material data together with the collapse loads, are of primary importance in the validation of the bridged crack model proposed in the present paper. Of course, the validity of Eqs. (16) and (17) is limited to the extent considered in the experimental program and does not include important parameters like the slenderness ratio λ_l.

4 NONLINEAR APPROACH TO FLEXURAL AND CRUSHING FAILURE

With respect to the previous proposed approach, some specific problems can be better investigated by considering the material nonlinearities. This is the case, for instance, of the phenomenon of hyper-strength typical of lightly RC beams, and the plastic rotational capacity of RC beams in presence of stirrups. Both these phenomena are largely influenced by the material nonlinearity, in tension and compression. On the other hand, differently from the problem of diagonal tension failure, in these cases the analysis can be limited to the study of the mid-span portion of the beam. To this aim, Carpinteri et al. [13] have developed a numerical procedure, based on nonlinear fracture mechanics models, that is briefly outlined in the following.

4.1 Numerical model

Let us consider a portion of a RC beam subjected to a constant bending moment, M (Fig. 9). This element, having a span to height ratio equal to unity, is representative of the zone of a beam where a plastic hinge formation takes place. Then, it is assumed that fracturing and crushing processes are fully localized along the mid-span cross section of the element, whereas the part of the hinge outside of the localization zone is assumed to be elastic. The loading process is characterized by crack propagation in tension, steel yielding and/or slippage, as well as concrete crushing in compression.

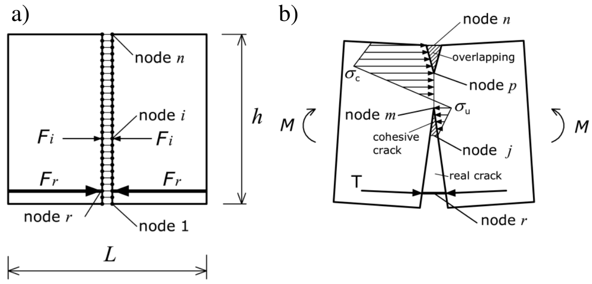

Figure 8: Central beam portion: (a) finite elements nodes; and (b) force distribution with cohesive crack in tension and crushing in compression.

The behavior of concrete in tension is described by means of the well-established cohesive crack model [21, 22]. The softening function, $\sigma=f(w)$, is considered as a material property, as well as the critical value of the crack opening, w_c, the fracture energy, $\mathcal{G}_F$, and the tensile strength, σ_u. A simple linear relationship has been adopted.

As far as modeling of concrete crushing failure is concerned, the overlapping crack model proposed by Carpinteri et al. [14] is adopted. According to such an approach, the inelastic and localized deformation in the post-peak regime is described by a fictitious interpenetration of the material, while the remaining part of the specimen undergoes an elastic unloading. In complete analogy with the cohesive crack model, the material properties are the compressive strength, σ_c, the crushing energy, $\mathcal{G}_C$, which is a dissipated surface energy, and the critical value for the relative interpenetration.

Finally, the steel reinforcement is modeled through concentrated forces applied at the crack faces, functions of the relative opening displacement. An elasto-perfectly plastic stress vs. crack opening relationship is used, derived from the bond-slip interaction between rebar and concrete.

The RC member is considered as

constituted by two symmetrical elements characterized by an elastic behavior, and connected by means of (n) pairs of nodes (Fig. 8a). In this approach, cohesive and overlapping stresses applied along the mid-span cross-section are replaced by equivalent nodal forces, F_i, by integrating the corresponding stresses over the nodal spacing. Such nodal forces depend on the nodal opening or interpenetration displacements according to the cohesive or overlapping softening laws.

With reference to Fig. 8a, the horizontal forces, F_i, acting at the i-th node along the mid-span cross section can be computed as follows:

$$\{F\} = [K_w]\{w\} + \{K_M\}M \tag{18}$$

where: $\{F\}$ is the vector of nodal forces, $[K_w]$ is the matrix of the coefficients of influence for the nodal displacements, $\{w\}$ is the vector of nodal displacements, $\{K_M\}$ is the vector of the coefficients of influence for the applied moment M.

Equation (18) constitutes a linear algebraic system of (n) equations and ($2n$+1) unknowns, $\{F\}$, $\{w\}$ and M. With reference to the generic situation reported in Fig. 8b, (n) additional equations can be introduced by considering the constitutive laws for concrete in tension and compression and for the reinforcement (see [14] for more details). The last additional equation derives from the strength criterion adopted to govern the propagation processes. At each step of the loading process, in fact, we can set either the force at the fictitious crack tip, m, or the force in the fictitious crushing tip, p, equal to the material strength, in tension or compression, respectively. Hence, the driving parameters of the process are the crack length and the crushing advancement. At each step of the algorithm, the localized beam rotation, ϑ, is calculated as a function of the nodal relative displacements and the applied bending moment, by means of elastic coefficients of influence.

4.2 Comparison between numerical predictions and experimental results

In this section, a comparison between the numerical predictions using the cohesive/overlapping crack model and the results of two experimental campaigns is presented. First, the three-point-bending tests carried out by Bosco et al. [23] on reinforced high-strength concrete beams to investigate the size effects on the minimum reinforcement percentage are considered. Three different size-scales were analyzed characterized by h=0.10, 0.20 and 0.40 m, and a constant width, b, equal to 0.15 m. The span to depth ratio was equal to 6. Five different steel percentages, ρ, were considered for each beam size. The material properties can be deduced from ref. [23]. In the numerical simulations, the RC element of Fig. 8 is assumed to be representative of the mid-span portion of the beam.

The numerical simulations compared to the corresponding experimental results, in terms of applied load vs. mid-span deflection curves, are shown in Fig. 9 for the beams with h=0.10 m. Such curves evidence a transition from an overall softening response to a hardening response by increasing the steel percentage, with the appearance of local snap-through instabilities. A comprehensive comparison between numerical and experimental results is reported in [15].

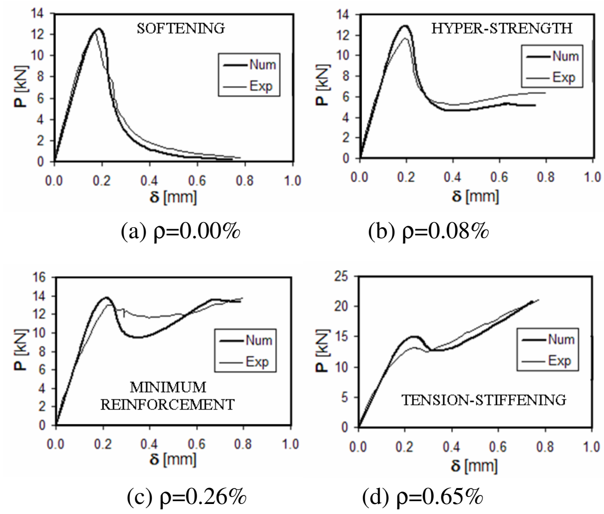

Figure 9: Comparison between numerical and experimental load vs. mid-span deflection curves for h=0.1 m and different amounts of reinforcement.

The second considered experimental campaign is that carried out by Bosco and Debernardi [24] to investigate the size effect on the rotational capacity of RC beams. In order to obtain a consistent comparison, the numerical simulations have been carried out by modeling the beam portion positioned at the mid-span of the beam. This element is characterized by a span to height ratio equal to one. The rotations of such a portion, where the largest amount of ductility is developed, were experimentally determined as functions of the applied bending moment. Numerical and experimental moment-rotation curves are compared in Fig. 10 for different beam heights and different steel percentages. Such diagrams put into evidence that the maximum rotation is a decreasing function of the tensile reinforcement ratio and of the beam height.

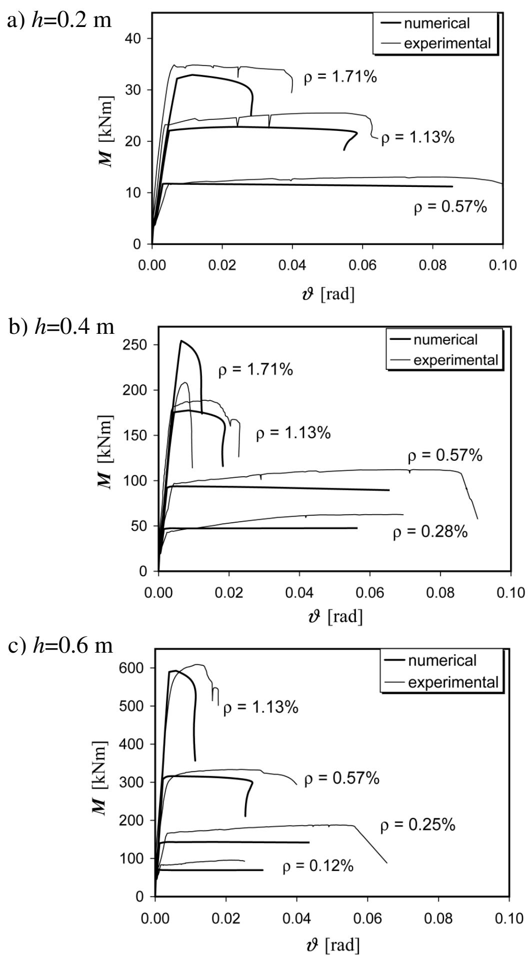

Figure 10: Comparison between numerical and experimental results for different beam heights.

In the case of low steel percentages, the mechanical behavior is characterized by the reinforcement yielding and the mechanical response is almost plastic. By increasing the reinforcement amount, the contribution of concrete crushing becomes more and more evident with the appearance of a softening branch at the end of the plastic plateau. This is an important feature of the proposed model, which also permits to follow snap-back branches by controlling the loading process through the length of the tensile crack or the extension of the crushing zone.

5 UPPER AND LOWER BOUNDS FOR DUCTILE RESPONSE

5.1 Minimum reinforcement percentage

In this section, a new expression for the minimum reinforcement amount is proposed on the basis of a wide parametric analysis [15]. To this aim, different values of the beam height, h, ranging from 0.10 and 3.20 m, and different values of the concrete compressive strength, σ_c, ranging from 16 to 76 MPa, have been considered. The yield strength and the elastic modulus of the steel reinforcement are σ_y=600 MPa and E_s=200 GPa, respectively. The ratio between effective and overall depth, d/h, is equal to 0.9. For each of the considered beams, several simulations have been carried out by varying the steel percentage, in order to find the minimum reinforcement amount. In particular, such a value is determined when the peak cracking load, P_{cr}, equals the ultimate load, P_u, as shown in Fig. 11.

When the flexural behavior of lightly RC beams is studied, according to the numerical model proposed in Section 4, the functional relationship among the quantities that characterize the phenomenon is:

$$M = \Phi\,(\sigma_u, \mathcal{G}_F, E_c, \sigma_y, \rho, h; \vartheta), \qquad (19)$$

where the parameters describing the behavior of concrete in compression, σ_c and $\mathcal{G}_C$, are not explicitly considered, since the crushing failure is not involved in the failure mechanism. On the other hand, only the beam height, h, is considered if the geometrical ratios of the samples, b/h and L/h, are assumed to be constant. The application of Buckingham's Π-Theorem for physical similarity and scale modeling permits to further minimize the dimension space of the primary variables by combining them into dimensionless groups. In case h and $\sqrt{\mathcal{G}_F E_c}$, which corresponds to the material toughness K_{IC}, are assumed as the dimensionally independent variables, the functional relationship becomes:

$$\frac{M}{h^{5/2}\sqrt{\mathcal{G}_\mathrm{F} E_\mathrm{c}}} = \Phi_1\left(\frac{\sigma_\mathrm{u} h^{1/2}}{\sqrt{\mathcal{G}_\mathrm{F} E_\mathrm{c}}}, \rho\frac{\sigma_\mathrm{y} h^{1/2}}{\sqrt{\mathcal{G}_\mathrm{F} E_\mathrm{c}}}, \vartheta\frac{E_\mathrm{c} h^{1/2}}{\sqrt{\mathcal{G}_\mathrm{F} E_\mathrm{c}}}\right), \tag{20}$$

that, in dimensionless form, is:

$$\tilde{M} = \Phi_1\left(s, N_P, \vartheta_\mathrm{n}\right), \tag{21}$$

where:

$$s = \frac{K_{IC}}{\sigma_\mathrm{u} h^{1/2}} \tag{22}$$

and N_P (Eq. (6)) are the governing nondimensional numbers, $\tilde{M}$ is the nondimensional bending moment, and ϑ_n is the normalized local rotation. As a result, each numerical simulation is completely described by a different couple of values s and N_P. In particular, the value of N_P relative to the condition of minimum reinforcement is referred to as $N_{P,L}$, where subscript L stands for "lower", since it will define the lower limit to the range of ductile response. The values of s and $N_{P,L}$ for the numerical simulations carried out in this study, are shown in Fig. 11. The obtained trend is described by the following hyperbolic curve:

$$N_{P,L} = 0.267\, s^{-0.70}. \tag{23}$$

By substituting Eqs. (6) and (22) into (23), the following expression for the minimum reinforcement amount is obtained:

$$A_\mathrm{s,min} = 0.267\frac{\sigma_\mathrm{u}^{0.70} K_\mathrm{IC}^{0.30}}{\sigma_\mathrm{y}} bh^{0.85} \tag{24}$$

The same calculations have been performed also for a T-beam with the flange in compression having the width equal to $8b$ and the height equal to $0.20h$. Such geometrical ratios determine a section modulus 1.5 times larger than that of a rectangular section having the same height and the width equal to b. The expression obtained for the minimum reinforcement area is:

$$A_\mathrm{s,min} = 0.339\frac{\sigma_\mathrm{u}^{0.84} K_\mathrm{IC}^{0.16}}{\sigma_\mathrm{y}} bh^{0.92} \tag{25}$$

The minimum reinforcement percentages, $A_\mathrm{s,min}/bd$, obtained from Eqs. (24) and (25) are compared to the prescriptions of the design codes in Fig. 12.

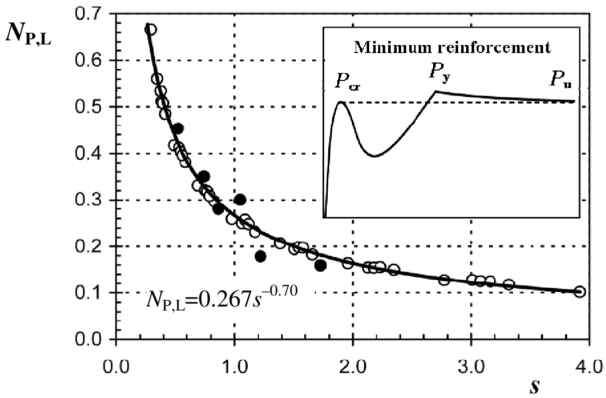

Figure 11: Best-fit relationship of numerical results (not filled-in symbols) between $N_{P,L}$ and s. Filled-in symbols refer to experimental results.

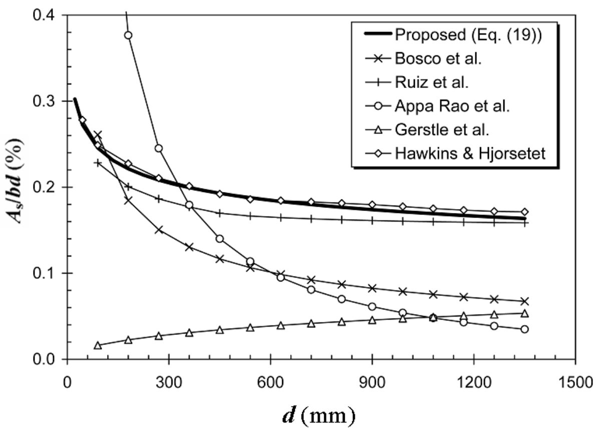

Figure 12: Comparison of minimum reinforcement ratios given by different codes for σ_c=35 MPa and σ_y=450 MPa.

5.2 Plastic rotation capacity

A second detailed numerical study is proposed to analyze the effect of each parameter to the plastic rotation capacity. With reference to the moment vs. rotation curves obtained by applying the proposed algorithm (Fig. 10), the plastic component of the total rotation is obtained as the difference between the rotation beyond which the moment starts descending rapidly and the rotation corresponding to the reinforcement yielding.

The results of several numerical simulations, carried out by considering different beam heights and reinforcement percentages, are summarized in the plastic rotation, ϑ_{PL}, vs. relative neutral axis position, x/d, diagram shown in Fig. 13. Such a diagram is consistent with the practical prescriptions of the Eurocode 2 [25] (dashed curve in Fig. 13). Beams with a height equal to 0.2 m have a rotational capacity greater than that suggested by the code. On the other hand, by increasing the beam height up to 0.8 m, the rotations provided by the code appear to be not conservative. It is worth noting that the numerical results for h=0.4 m are in good agreement with the curve provided by the code, which represents the 5%-fractile of the plastic rotations of beams or slabs with height of about 0.3 m (see [11] for more details).

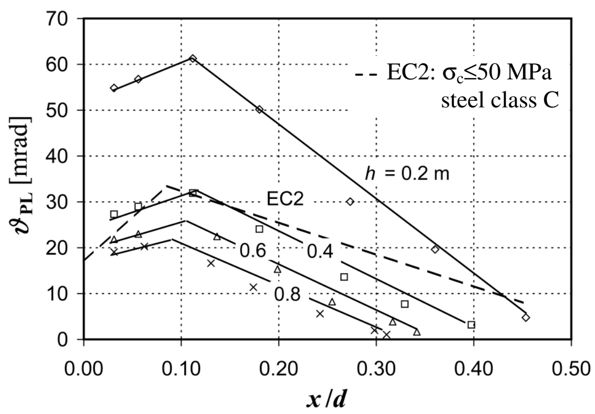

Figure 13: Predicted plastic rotation for different beam heights (solid lines) compared with the Eurocode 2 prescription (dashed line).

It is evident from the diagrams in Fig. 13 that the plastic rotation capacity tends to zero as the neutral axis relative position coordinate increases, i.e. the tensile reinforcement percentage increases. In particular, it is possible to define an upper limit to the reinforcement amount beyond which the steel does not yield, and the beam collapses in compression, without the development of a significant ductility. Such a limit, function of all the variables involved in the phenomenon, can be obtained by means of dimensional analysis, as previously done for the minimum reinforcement. In this case, since we are interested in over-reinforced concrete beams, h and $\sqrt{\mathcal{G}_C E_c}$ are assumed as the dimensionally independent variables, whereas the parameters describing the behavior of concrete in tension, σ_u and $\mathcal{G}_F$, are omitted. The beams considered in the previous section for the evaluation of the minimum reinforcement are now analyzed in case of large reinforcement amount. In particular, for each of the beams, several numerical simulations have been carried out in order to find the limit value of the reinforcement percentage beyond which the steel does not yield. The best fitting relation relating the upper bound for the reinforcement amount to the mechanical and geometrical parameters of the beam is:

$$A_{s,\max} = 0.25 \frac{\sigma_c^{0.49} \left(\sqrt{\mathcal{G}_C E_c}\right)^{0.51}}{\sigma_y} b h^{0.75} \tag{26}$$

6 CONCLUSIONS

The two approaches proposed to analyze the behavior of RC beams with and without stirrups share most of the governing parameters, included in the different nondimensional numbers adopted (N_P, N_C, s, λ_l). Therefore, the obtained results can be combined, and the conditions for the structural design of RC elements exhibiting ductile response can be derived. From a qualitative point of view, the decrease in one parameter among h, ρ, and σ_y, or the increase in σ_u or $\mathcal{G}_F$, all the other parameters being kept constant, determines a transition from ductile response to unstable tensile crack propagation, as represented in Fig. 14. On the other hand, the increase in h, or ρ, or σ_y, or the decrease in σ_c or $\mathcal{G}_C$, all the other parameters being kept constant, produces a transition towards crushing failure without steel yielding (Fig. 14). The intermediate range is characterized by a ductile behavior with the development of significant plastic rotations for RC beams with stirrups, or a brittle shearing failure in the case of beams without stirrups.

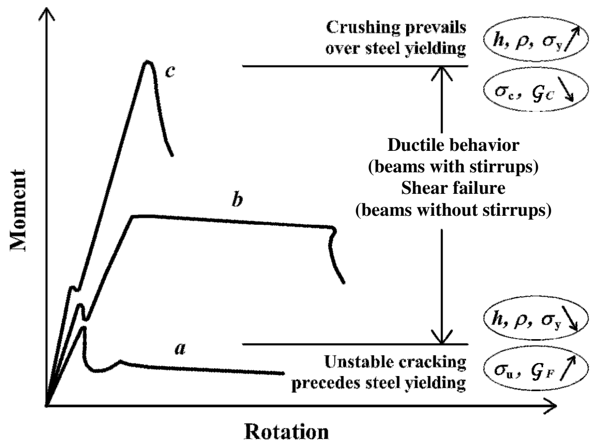

Figure 14: Conditions for structural design of RC members with ductile response.

AKNOWLEDGEMENTS

The Authors acknowledge the financial support of the Italian Ministry of Education, University and Research to the project “Advanced applications of fracture mechanics for the study of integrity and durability of materials and structures” within the PRIN program for the year 2008.

REFERENCES

[1] Gustafsson, P. and Hillerborg, A., 1988. Sensitivity in shear strength of longitudinally reinforced concrete beams to fracture energy of concrete. *ACI Struct. J.* **85**:286-94.

[2] Niwa, J., 1997. Size effect in shear of concrete beams predicted by fracture mechanics. *CEB Bulletin d'Information* **137**:147-58.

[3] Jenq, Y.S. and Shah, S.P., 1989. Shear resistance of reinforced concrete beams - A fracture Mechanics approach. In Li, V. and Bažant, Z.P., (eds.), *Fracture Mechanics: Applications to Concrete*, American Concrete Institute, Detroit, pp. 237-58.

[4] So, K.O. and Karihaloo, B., 1993. Shear capacity of longitudinally reinforced beams - A fracture mechanics approach. *ACI Struct. J.* **90**:591-600.

[5] Carpinteri, A. (ed.) 1999. *Minimum Reinforcement in Concrete Members*. Elsevier Science Ltd.

[6] Hawkins, N.M. and Hjorsetet, K., 1992. Minimum reinforcement requirements for concrete flexural members. In Carpinteri A. (ed.), *Applications of Fracture Mechanics to Reinforced Concrete*, Elsevier Applied Science, London, pp. 379-412.

[7] Ruiz, G., 2001. Propagation of a cohesive crack crossing a reinforcement layer. *Int. J. Fract.* **111**:265-82.

[8] Eligehausen, R. and Langer P., 1987. Rotation capacity of plastic hinges and allowable moment redistribution. *CEB Bulletin d’Information* **175**: I 7.9-I 7.27.

[9] Hillerborg, A., 1990. Fracture mechanics concepts applied to moment capacity and rotational capacity of reinforced concrete beams. *Eng. Fract. Mech.* **35**:233-40.

[10] Bigaj, A.J. and Walraven, J., 2002. Size effects on plastic hinges of reinforced concrete members. *Heron* **47**:53-75.

[11] Eligehausen, R., Fabritius, E., Li, L. and Zhao, R., 1993. An analysis of rotation capacity tests. *CEB Bulletin d’Information* **218**:251-73.

[12] Carpinteri, A., 1984. Stability of fracturing process in RC beams. *J. Struct. Eng.***110**:544-58.

[13] Bosco, C. and Carpinteri, A., 1992. Softening and snap-through behavior of reinforced elements. *J. Eng. Mech.* **118**: 1564-77.

[14] Carpinteri, A., Ruiz Carmona, J. and Ventura G., 2011. Failure mode transitions in reinforced concrete beams – Part 1: Theoretical model. *ACI Struct. J.* **108**:277-85.

[15] Carpinteri, A., Corrado, M., Mancini, G. and Paggi, M., 2009. Size-scale effects on plastic rotational capacity of reinforced concrete beams. *ACI Struct. J.* **106**:887-96.

[16] Carpinteri, A. and Corrado, M., 2011. Upper and lower bounds for structural design of RC members with ductile response. *Eng. Struct.* **33**:3432-41.
[17] Tada, H., Paris, P. and Irwin, G., 1963. *The stress Analyses of Cracks Handbook*. Paris Productions Incorporated.
[18] Portela, A. and Aliabadi, M. H., 1992. Crack Growth Analysis Using Boundary Elements. *Comput. Mech. Publications*.
[19] Carpinteri, A., Ferro, G. and Ventura, G., 2004. Double brittle-to-ductile transition in bending of fibre reinforced concrete beams with rebars. *Int. J. Num. Anal. Methods Geomech.* **28**:737-56.
[20] Carpinteri, A., Ruiz Carmona, J. and Ventura G., 2011. Failure mode transitions in reinforced concrete beams – Part 2: Experimental tests. *ACI Struct. J.* **108**:286-93.
[21] Hillerborg, A., Modeer, M. and Petersson, PE., 1976. Analysis of crack formation and crack growth in concrete by means of fracture mechanics and finite elements. *Cement and Concrete Res.* **6**:773-82.
[22] Carpinteri, A., 1989. Cusp catastrophe interpretation of fracture instability. *J. Mech. Phys. Solids* **37**:567-82.
[23] Bosco, C., Carpinteri, A. and Debernardi P.G., 1990. Minimum reinforcement in high-strength concrete. *J. Struct. Eng.* **116**:427-37.
[24] Bosco, C. and Debernardi, P.G., 1993. Influence of some basic parameters on the plastic rotation of reinforced concrete elements. *CEB Bulletin d'Information* **218**:25-44.
[25] CEN TC/250, 2004. *Eurocode 2: Design of Concrete Structures, Part 1-1: General Rules and Rules for Buildings*.